ARTICLE NO. 79-0345R

J80-015

Investigation of Crossflow Shocks on Delta Wings in Supersonic Flow

20005
20015
20017

Michael J. Siclari*
Grumman Aerospace Corporation, Bethpage, N.Y.

In the study described, a finite difference approach to solving the rotational Euler equations, explicitly fitting shocks as a boundary, is applied to a variety of geometrical shapes in the lower supersonic Mach number regime. It is shown how special techniques based on the physics of the flow can be used to circumvent a variety of numerical difficulties encountered with the conical flow problem that are primarily associated with the initial value characteristics of the hyperbolic scheme, causing embedded shock-induced entropy and crossflow layers to develop on the body surface.

Introduction

NUMEROUS investigations over the past several decades have dealt with the problem of supersonic flow over thin wings. Many of the earlier methods used linearized potential flow theory and slender body assumptions to obtain solutions. The failure of linearized potential flow solutions for flows where significant supersonic crossflow regions exist is fairly well known (e.g., Refs. 1-3). More recently, nonlinear methods, such as the method of characteristics[4] and the method of lines,[5] were developed which were adequate at small angles of attack and simple, but not very thin, cross-sectional shapes. Nevertheless, these nonlinear methods did not broach the topic of crossflow embedded shocks which occur on thin bodies, even at relatively small angles of attack. Under certain geometric and flow conditions, a large expansion occurs around the leading edge, causing an embedded region of supersonic crossflow to occur on the leeward side of the body. Since the supersonic region has no advance warning of the symmetry plane crossflow stagnation condition, an embedded shock forms, causing the crossflow to become subsonic and capable of satisfying this boundary condition.

A shock-capturing finite-difference approach was developed and applied to complex shapes with embedded shocks in the high supersonic to hypersonic Mach number regime.[6,7] This shock-capturing approach uses the conservation form of the Euler governing equations in order to resolve the embedded shocks with a minimal amount of numerical instability.

In contrast to the aforementioned nonlinear methods integrating the rotational form of Euler equations, a technique was developed to integrate the irrotational equations for supersonic conical flow. A relaxation method was applied to the conical full potential flow equation in Ref. 3 that relied heavily on numerical transonic techniques. Numerical solutions were computed successfully for circular/elliptic cones and thin winglike cross sections from low to high incidence at freestream Mach numbers between 1.2 and 3. This method captures the shocks over a few mesh points, apparently without numerical instabilities. Using the nonlinear potential flow equations also precludes any difficulties with vortical singularities or layers.

Very few studies using the rotational Euler governing equations have reported obtaining results for thin elliptical cones or delta winglike shapes at moderate incidence and Mach numbers less than 3.0.

The present investigation involves the application of the methods developed in Refs. 10 and 11 to generate solutions to the three-dimensional rotational Euler equations focusing on the aforementioned geometries. The numerical method basically consists of a hyperbolic marching two-level predictor-corrector finite-difference integration scheme, along with explicit "shock as a boundary" fitting techniques. Conformal mappings are applied to the cross-sectional geometry in planes transverse to the marching direction. This procedure was first suggested by Moretti[10] for three-dimensional flow. In Ref. 12, a preliminary application of these techniques to conical delta wings with embedded shocks showed promise with certain areas needing further investigation. The conical flow problem supplies a convenient check on the procedures, since the same solution exists in each crossflow plane; whereas a fully three-dimensional problem is indeed difficult to validate. Certain instabilities in the numerical computation of conical crossflow shocks required further study and a numerical technique allowing resolution of the vortical singularities or layer needed to be established. These topics are the intent of the present study, as well as the application of these techniques to the lower supersonic Mach number regime and a discussion of the difficulties encountered in obtaining converged solutions.

Conical flow solutions to the Euler equations were also used as starting solutions for the flow over three-dimensional delta wings.

Conical Flow

Initial Starting Plane Solutions

Since a hyperbolic marching technique is used to integrate Euler's equations, an initial starting solution is required. The computation of the flowfield about thin delta wing cross sections was desired. Unfortunately, using a circular cone solution limits the conical wing solutions to those planform angles and angles of attack at which approximate circular cone solutions exist. In order to eliminate this restriction, and the added complexity of having to deform the circular cone geometry to the desired cross section, the linearized potential flow solution was initially used as a starting solution.

Crossflow Shock Detection

Several problems arose in the detection of crossflow shocks at the lower freestream Mach numbers ($M_\infty \sim 2.0$). At these Mach numbers, a limited zone (bubble) of supersonic

Presented as Paper 79-0345 at the AIAA 17th Aerospace Sciences Meeting, Huntsville, Ala., Jan. 15-17, 1979; submitted Feb. 28, 1979; revision received July 2, 1979.

Index categories: Supersonic and Hypersonic Flow; Computational Methods; Shock Waves and Detonations.

*Senior Research Scientist.

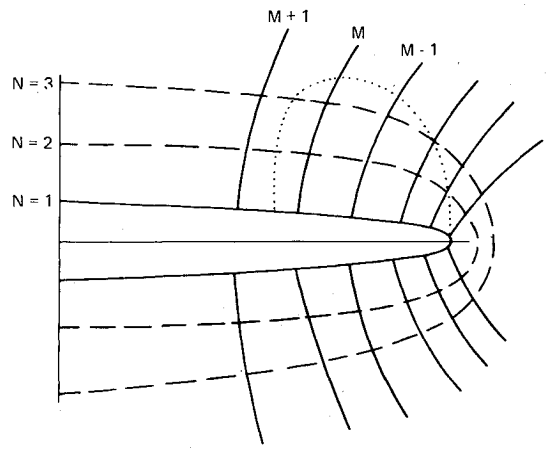

Fig. 1 Mapped grid lines.

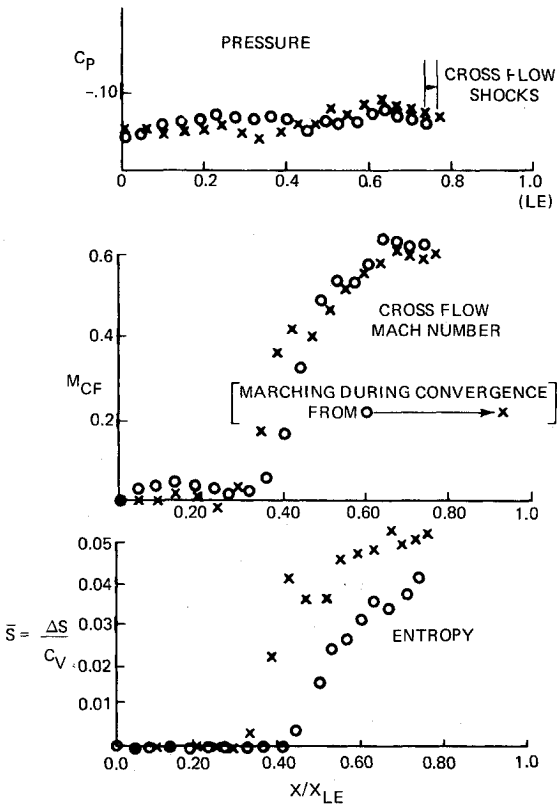

Fig. 2 Development of leeward surface vortical singularity.

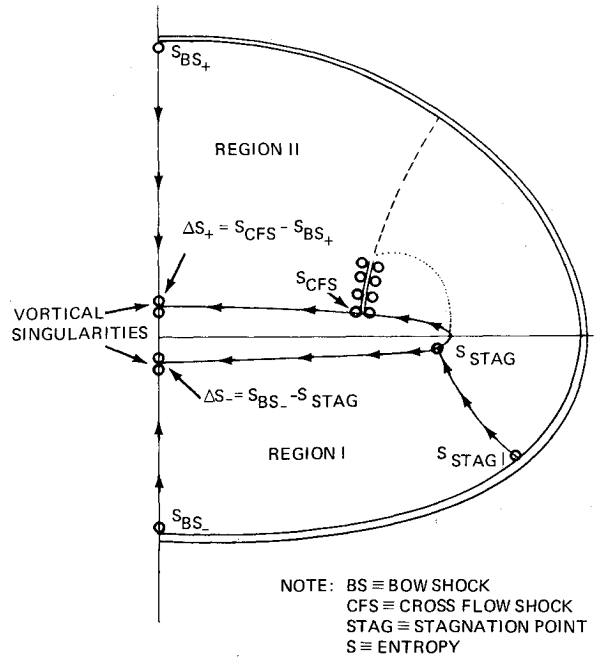

Fig. 3 Basic sketch of flowfield.

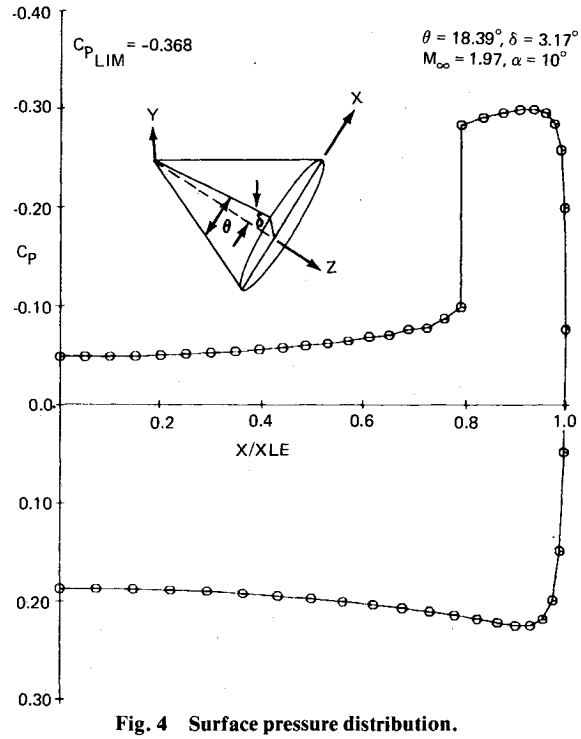

Fig. 4 Surface pressure distribution.

crossflow exists on the leeward side of the body. To insure the proper detection and placement of crossflow shock points, a condition that the crossflow upstream of the shock must be supersonic was imposed. The crossflow shock becomes a continuous extension of the upstream sonic line and its strength decays radially outward from the body. As the shock becomes weak, it's shape basically follows the shape of the sonic line. The computational scheme assumes the shock is an M grid line boundary (see Fig. 1a). If weak crossflow shock points are detected whose shape significantly differs from the shape of an original M-grid line developed from the mapping, the original near orthogonality of the crossflow plane mesh will be disturbed, leading to an unstable computation and spurious numerical results. Thus, a shape criterion was imposed to eliminate this problem and retain a reasonable grid line arrangement.

During the iterative marching to a conical solution, several transient phenomena occurred pertaining to the shape of the crossflow shock that led to instabilities in the computation. In the field, the normal vector to the shock is computed by an iterative technique that satisfies both the Rankine-Hugoniot conditions and the characteristic equation downstream of the shock, with the slope of the shock in the crossflow plane being computed numerically from the shock position. On the body, the shock is computed normal to the surface in order to satisfy the body boundary condition. Applying this technique revealed a displacement between the body shock location and the location of the field shock points. Hence, using numerical derivatives for the shock shape in the crossflow plane led to instabilities in the shock shape, which caused the field shock points to eventually move into the supersonic region with zero strength.

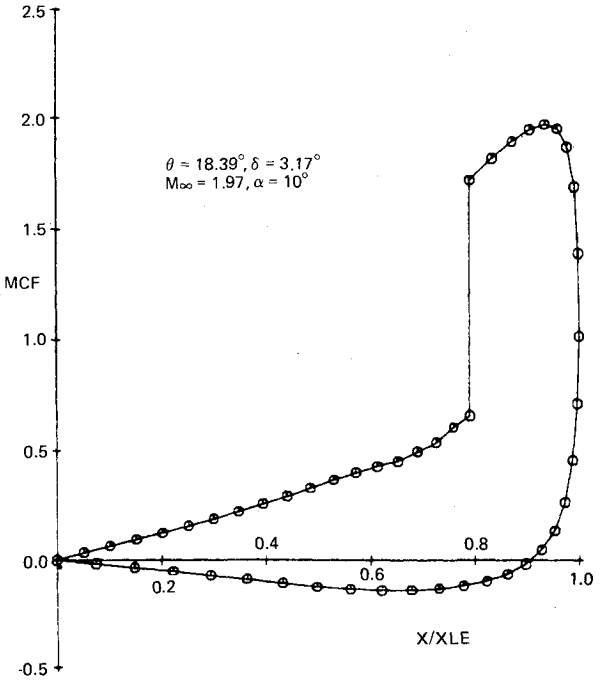

Fig. 5 Crossflow Mach number distribution.

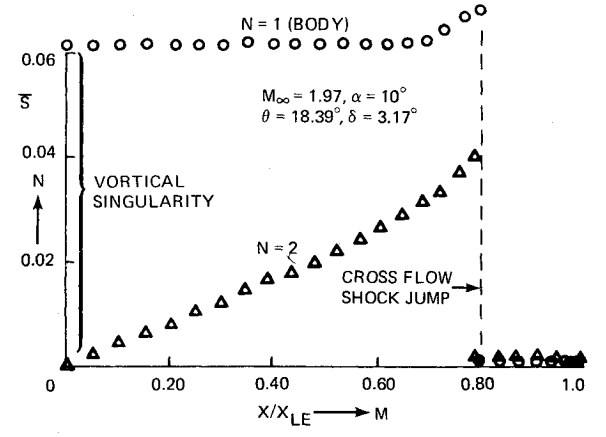

Fig. 6 Leeward entropy distribution.

To circumvent this problem, a condition was imposed on the field shock points such that their normal vectors would approximately lie in the direction of the N grid lines or crossflow direction. Thus, the field shock points were computed as normal shocks relative to the local crossflow velocity independent of its radial shape and became affixed along the transient sonic line promoting stabilization of the shock position. It was also found that once convergence was achieved (i.e., the shock shape being nearly normal), the numerical shock normals could be imposed again with very little or no change in the results. The reasons for this transient behavior of the shock shape are discussed in the following section.

Vortical Layer

During the iterative marching to a conical solution, certain problems arose in the flow variables computed on the body between the crossflow shock and leeward symmetry plane. Severe oscillations developed in this region as soon as the crossflow shock approached convergence strength. To determine the problem, a large number of grid points was inserted in this region to allow for the resolution of any steep gradients in flow variables. Figure 2 shows a typical

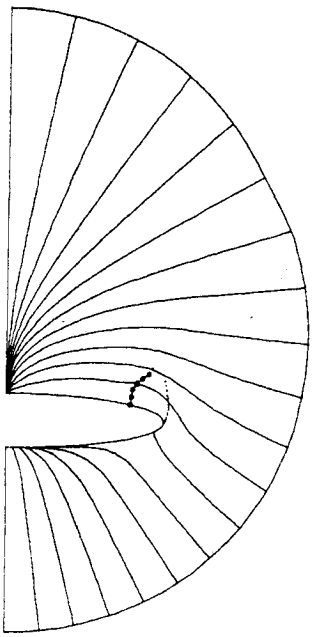

Fig. 7 Crossflow streamline pattern, $\theta = 18.39$ deg, $\delta = 3.17$ deg, $M_\infty = 1.97$, $\alpha = 10$ deg.

distribution of pressure, crossflow Mach number, and entropy that results in the region between the crossflow shock and leeward symmetry plane. A large gradient in entropy and crossflow Mach number is revealed. Near the shock, the entropy corresponds to the entropy being developed by the shock and, at the symmetry plane, the entropy is still negligible corresponding to its initial prescribed value. Thus, a wave in entropy and crossflow developed by the shock was slowly traveling toward the leeward symmetry plane. The gradients in entropy and crossflow were also causing oscillations in pressure. Since the body surface is a streamline, the entropy produced by the crossflow shock must propagate to the symmetry plane, thus constituting the vortical singularity. The computation was allowed to proceed, in the hope that the entropy would propagate to the symmetry plane, but the process turned out to be too slow, since the entropy propagates at roughly the crossflow velocity and thus becomes an asymptotic process.

Even if the entropy propagated to the symmetry plane, a discontinuity in entropy would result which cannot be resolved numerically. Figure 3 shows a basic sketch of the vortical singularities and the entropy field occurring for a thin ellipse with a crossflow shock. Nodal singularities occur at the body surface in both symmetry planes. A saddle point also occurs on the windward side of the body near the leading edge. All three points correspond to crossflow stagnation points. The entropy on the surface of the body between the windward symmetry plane and low-pressure side of the crossflow shock comes from the saddle point or crossflow stagnation streamline which wets the body and originates at the bow shock. The entropy on the body in region II is generated by the crossflow shock.

The vortical singularities arise out of the coalescence of the crossflow streamlines at the body surface windward and leeward symmetry plane nodal points. The dividing streamline is the crossflow stagnation streamline in the vicinity of the leading edge. Thus, the entropy becomes multivalued at both nodal singularities. The discontinuity in entropy at the leeward symmetry plane is bounded by the surface streamline entropy that originates at the crossflow shock and the entropy of the symmetry plane streamline that originates at the leeward bow shock. The entropy of the windward vortical singularity is bounded by the entropy of the crossflow stagnation streamline at the saddle point and the entropy of

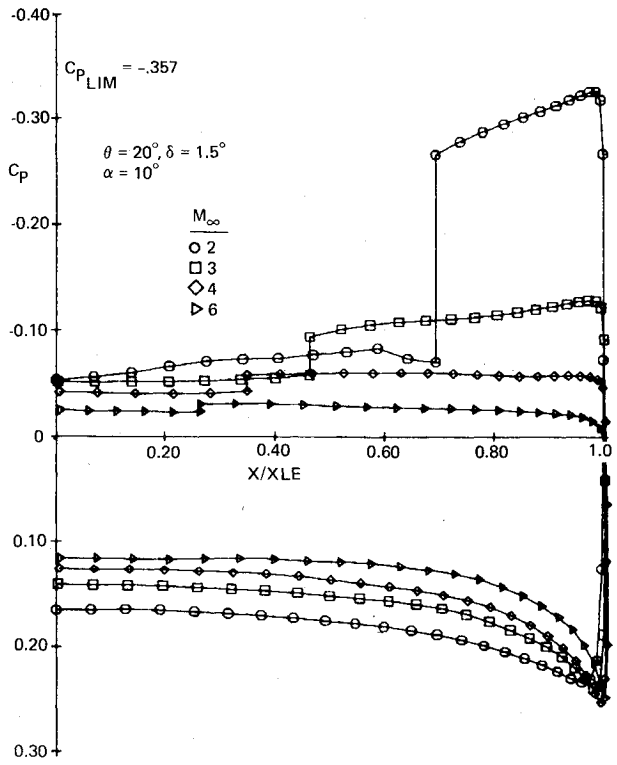

Fig. 8 Comparison of surface pressure distributions for different freestream Mach numbers.

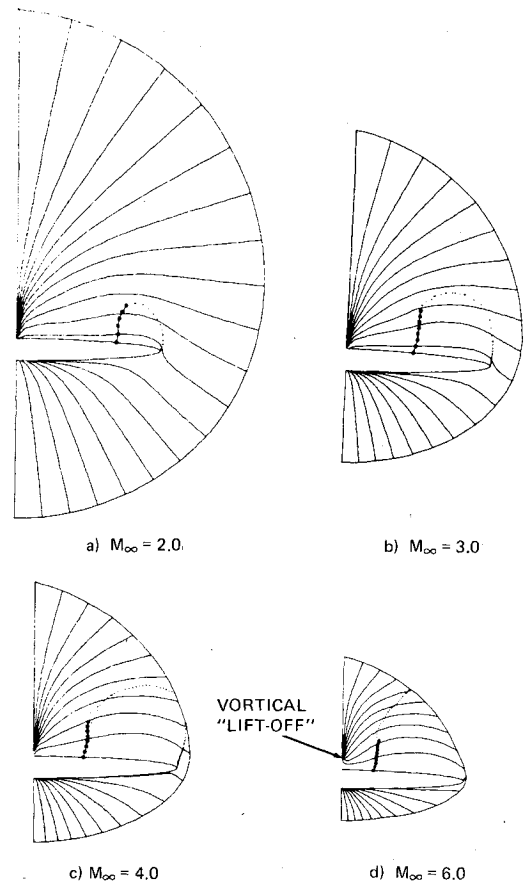

Fig. 9 Crossflow streamline pátterns, $\alpha = 10$ deg, $\theta = 20$ deg, $\delta = 1.5$ deg.

the windward symmetry plane streamline coming from the bow shock. The presence of a crossflow shock causes the leeward symmetry plane nodal singularity to be the foremost problem.

Consequently, a vortical layer is developed on the body surface which cannot be evaluated numerically by conventional techniques. This vortical layer also causes large radial gradients in entropy at the body surface which become infinite at both nodal singularities.

To circumvent the difficulties involved with the vortical layer and to speed up the process of the entropy and crossflow development on the body surface, several artifices had to be adopted based on the physics of the flow. The artifices are gradually removed as convergence is achieved.

The entropy development on the body is a true layer in that it is distinguishable from the rest of the flowfield as the surface streamline entropy, and thus develops singularities at the nodal points. The crossflow, on the other hand, is not a true layer, but it exhibits similar behavior. The layer in crossflow can be resolved numerically if a fine grid is used in the region between the crossflow shock and the symmetry plane. On the other hand, an artifice can be applied to make the crossflow linear between the value at the shock and zero at the symmetry plane at specified intervals during the iteration. Eventually, the gradient would reduce and then disappear as the flowfield converged.

Windward numerical differencing in the radial direction was imposed at the first N or circumferential mesh ring off the body to avoid differencing across the body layer where the steep radial gradients and discontinuities occur. The entropy on the body between the crossflow shock and leeward symmetry plane was set equal to the entropy of the high-pressure side of the shock. The entropy of the rest of the body was extrapolated from the crossflow stagnation streamline. All other circumferential mesh rings off the body are still computed using central-difference formulas. The advancement of the entropy on the body surface is only done when the crossflow shock nears convergence strength. The entropy on the body is then set to the aforementioned values and the computation is allowed to proceed. If the entropy changes significantly, the new values are reassigned to the body and the computation proceeds until reasonable convergence has been achieved.

To eliminate the oscillations in pressure as a result of the unresolved gradients, a one-step numerical damping or artificial viscosity was imposed in the region and the calculation restarted. Pressure and crossflow Mach numbers are shown in Figs. 4 and 5. A typical converged result for the entropy on the leeward body surface is shown in Fig. 6. As indicated, when these various procedures were adopted, the results improved markedly. Both the pressure and crossflow are smooth and the oscillations do not recur. The entropy distribution exhibits a discrete jump, representing the leeward vortical singularity from the body surface to the first field ring. In other words, the vortical singularity is smeared over one mesh point.

Discussion of Conical Results

Elliptic Cones at Moderate Incidence

Figure 4 shows the surface pressure coefficient distribution and crossflow shock computed for a 6:1 elliptic cone with subsonic leading edge at $M_\infty = 1.97$, $\alpha = 10$ deg. Figure 5 shows the corresponding surface crossflow Mach number distribution. Three crossflow stagnation points are readily apparent—two occurring in the symmetry planes, the third near the leading edge at approximately 91% of the span. A rapid acceleration and resulting expansion occurs around the leading edge in the direction of the leeward plane. The crossflow attains a sonic velocity before reaching the leeward side of the body. The crossflow then decelerates compressing the flow slightly and is finally shocked down to a subsonic value. The jump across the shock corresponds to the normal shock conditions governed by the crossflow Mach number

ahead of the shock. An approximately linear deceleration of the crossflow occurs between the shock and leeward symmetry plane. Figure 7 shows the resulting crossflow streamline pattern obtained by integration of the converged numerical data using a marching technique starting at the bow shock. Also shown are the crossflow and bow shocks and the numerically interpolated sonic line. The crossflow stagnation streamline is clearly indicated and designates the dividing streamline in the crossflow plane. All of the streamlines to either side of this coalesce at the nodal or vortical singularities. The windward streamlines appear to coalesce tangentially to the body at the windward vortical singularity, while the leeward streamlines coalesce normal to the leeward vortical singularity. The large expansion around the leading edge is depicted by the curvature of the streamlines and also by their origin at the bow shock. A slight inflection occurs in the leeward bow shock designating the approximate position where the leeward Mach cone merges into a finite strength bow shock. The proximity of the stagnation streamline to the leading edge is a good indicator of the degree of expansion that will occur around the leading edge.

The flowfield about a thinner elliptic cone, $\theta = 20$ deg and $\delta = 1.5$ deg, was computed for freestream Mach numbers of 2, 3, 4, and 6 at $\alpha = 10$ deg. These freestream conditions correspond to subsonic, near sonic or slightly supersonic, and supersonic leading edges, respectively. Figure 8 shows a comparison of the surface pressure coefficient for all four Mach numbers.

As the freestream Mach number increases, the crossflow shock moves inboard toward the leeward symmetry plane and the jump in pressure coefficient decreases.

It is interesting to note that the largest expansion in crossflow occurs for the lowest freestream Mach number corresponding to a subsonic leading edge. The crossflow stagnation point clearly moves closer to the leading edge with increasing Mach number. The character of the crossflow changes as the leading edge becomes increasingly supersonic and a recompression in crossflow occurs after expansion around the leading edge at $M_\infty = 6$. Figure 9 shows a comparison of the crossflow streamline patterns nondimensionalized to the same scale. A small region or bubble of supersonic crossflow exists at Mach 2. The bubble increases in extent with increasing Mach number until, at Mach 4, the bubble opens up and intersects the bow shock forming two distinct sonic lines. At Mach 6, remnants of the bubble are nonexistent and a large region of supersonic crossflow exists in the leeward plane bounded by the crossflow shock and sonic lines. The streamline pattern at Mach 6 indicates that the leeward vortical singularity is just slightly removed from the body.

It becomes readily evident why the low, supersonic, freestream Mach number cases are more difficult to compute numerically. The supersonic crossflow region becomes much smaller relative to the entire flowfield for the lower Mach numbers. In addition, the surface Mach numbers are comparable or even higher, causing the radial gradients to be much larger and more difficult to resolve with less available grid points.

Elliptic Cones, Low Incidence

Figures 10 and 11 show the pressure coefficient and crossflow Mach number distributions, respectively, for 15, 20, and 30 deg elliptic cones at $M_\infty = 2.0$, $\alpha = 5$ deg. The 15 and 20 deg wings correspond to subsonic leading edges with $a/b \sim 14$. The 30-deg wing corresponds to a sonic leading edge and a slightly thinner cross section $a/b \sim 16.5$. A strong crossflow shock occurs close to the leading edge for the most subsonic case even at this low incidence. As the planform or cone angle increases, the shock moves inboard and decreases rapidly in strength. The sonic leading edge, even though the crossflow was supersonic, exhibited only a very moderate compression; thus, it was not necessary to fit a shock. The

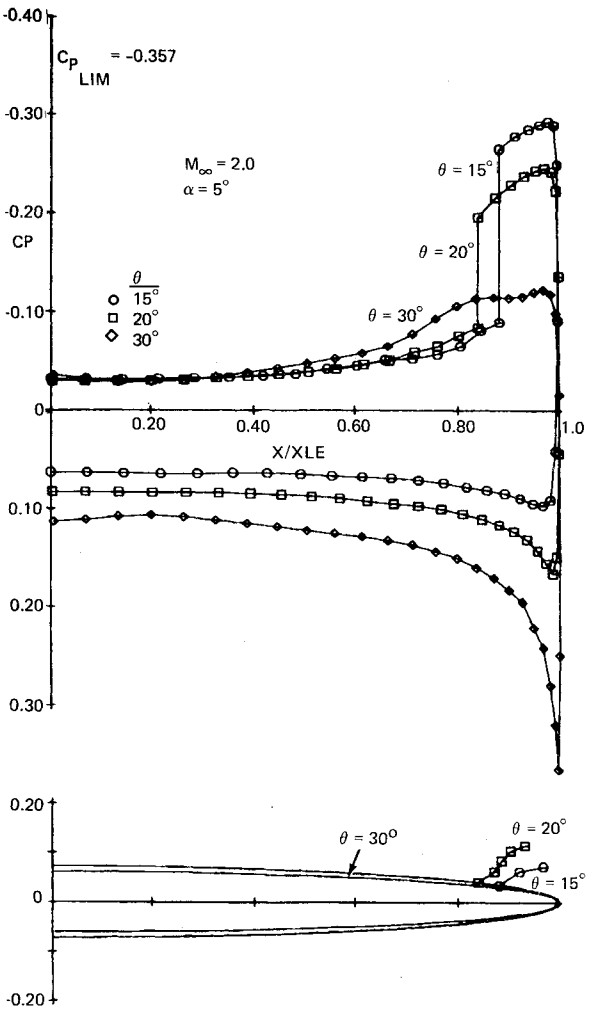

Fig. 10 Comparison of surface pressure distributions at low α.

leeward symmetry plane pressures are not affected significantly at the different planform angles. On the other hand, higher pressures occur on the entire lower surface as the planform angle increases. The sonic leading edge exhibits a very large compression at the lower surface leading edge. As the planform angle decreases or becomes more subsonic, the supersonic region extends less into the flowfield even though the surface Mach numbers become larger, corresponding to a stronger shock. The size of the shock is minute compared to the entire flowfield for the most subsonic case, and was very difficult to resolve with only three grid points to determine it. For these cases, 40 radial grid points were used, whereas 35 points were used at moderate incidence. Almost all the solutions were obtained using 45-50 circumferential mesh points.

Cones at High Incidence

Some examples of the flow generated by circular cones at high incidence were computed to determine if significant lift-off of the vortical singularity could be achieved at low supersonic Mach numbers. Figure 12 shows the crossflow streamline pattern computed for a 5 deg cone semiapex angle at $M_\infty = 2.0$, $\alpha = 10$ deg. The streamlines clearly depict the lift-off of the vortical singularity. The circular cone streamline pattern is distinct from the elliptic cone in that only one nodal singularity occurs in the leeward symmetry plane. The stagnation streamline wetting the body lies in the windward symmetry plane. Hence, the body windward symmetry plane point is the saddle point. Numerical difficulties were not encountered in computing this case because of the small cone angle. A supersonic crossflow region does not occur; thus, the

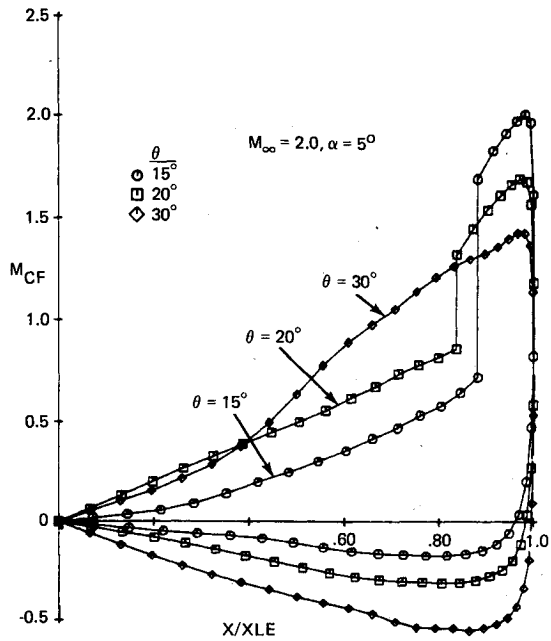

Fig. 11 Comparison of crossflow Mach number distributions at low α.

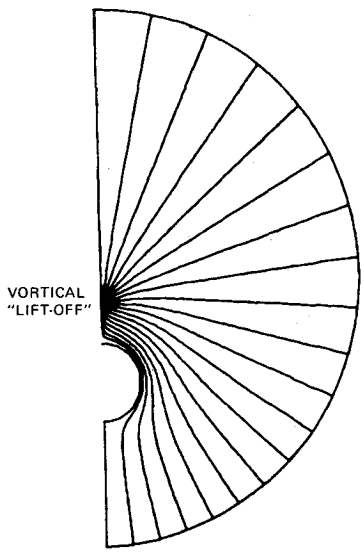

Fig. 12 Circular cone crossflow streamline pattern, $M_\infty = 2.0$, $\alpha = 10$ deg, $\theta = 5$ deg.

absence of a crossflow shock. The bow shock is weak and thus the flow is not far from irrotational.

Wing-Body Effect

To determine the interference effect of a conical body on a wing flowfield, conical wing-body geometries were computed. The centerbodies were cubicly faired to the wing at a specified conical location. The wing-body geometries were computed using a converged Euler solution for the wing as the initial starting solution. The geometry was then deformed continuously until the specified conical wing-body geometry was achieved, at which point in the marching technique the wing-body geometry was held invariant and conical until convergence was achieved.

The presence of the faired body pushes the location of the crossflow shock outboard toward the leading edge. The crossflow shock thus reacts earlier to the presence of the low values of crossflow that occur in the leeward shoulder region or wing-body juncture. The presence of the body increases the

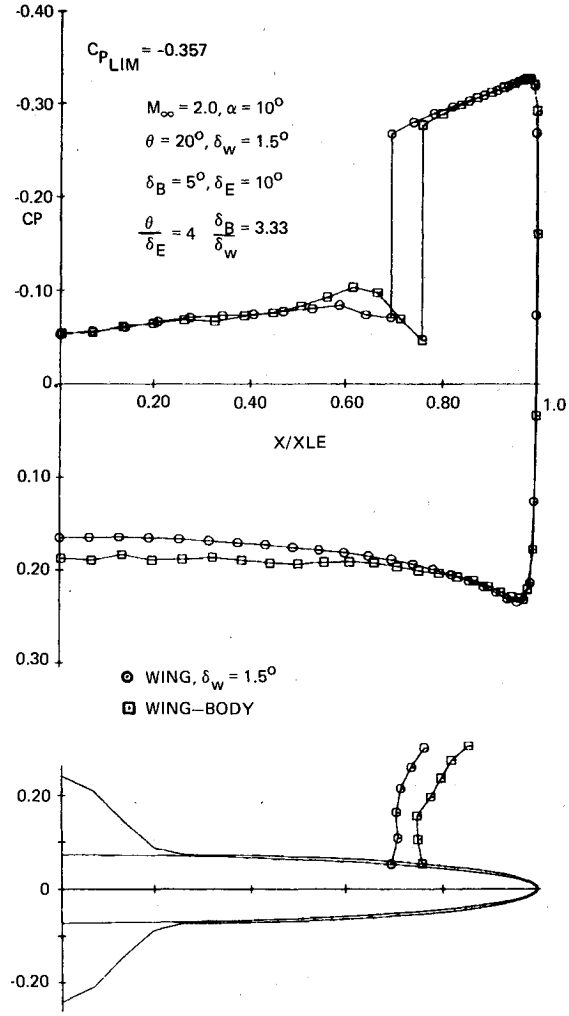

Fig. 13 Body interference effect on surface pressure distribution, $M_\infty = 2.0, \theta/\delta_E = 4, \delta_B/\delta_W = 3.333$.

windward pressures, but also increases somewhat the leeward pressures between the shock and symmetry plane. The outboard movement of the shock reduces the lift in the leeward expansion region. The crossflow streamline pattern changes somewhat in that the leeward streamlines appear to coalesce tangentially to the body at the vortical singularity, whereas the wing alone appeared to coalesce normal.

Figures 13 and 14 show the computed results for a not so blended wing-body combination. The body was faired to the wing at a 5 deg angle, δ_E, with a body centerline angle of 5 deg, δ_B, and the wing thickness angle remaining at 1.5 deg.

An interesting aspect of this flowfield is that the crossflow streamline pattern (Fig. 14) shows that the windward nodal or vortical singularity has moved off the symmetry plane and occurs at the wing-body juncture. The windward symmetry plane must remain a crossflow stagnation point, but becomes a saddle point instead of a nodal singularity.

The leeward vortical singularity remains intact and once again the streamlines appear to converge tangentially. Therefore, the leeward streamlines locally behave in a similar fashion to the leeward streamlines on a circular cone at moderate incidence. Similar behavior of the leeward nodal singularity for conical wing-body configurations has been observed in the nonlinear potential flow solutions[13] using the methods developed in Ref.3.

It must be mentioned that the conformal mapping clusters point around the leading edge of the wing. Hence, minimal resolution was obtained in the wing-body juncture area with fifty circumferential points.

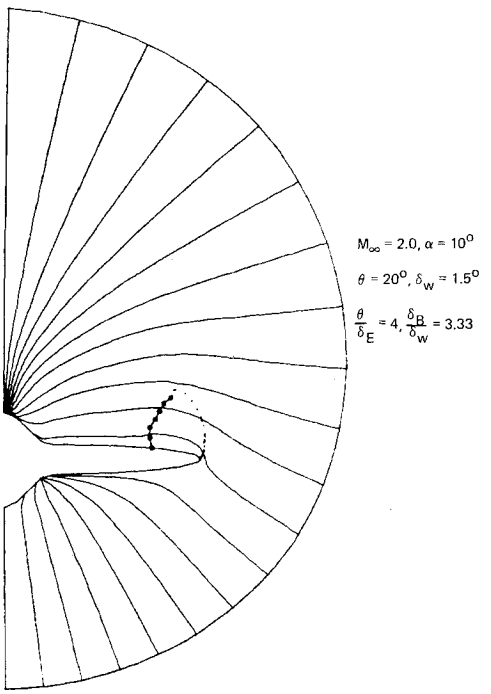

Fig. 14 Wing-body crossflow streamline pattern, $M_\infty = 2.0$, $\theta/\delta_E = 4, \delta_B/\delta_W = 3.333$.

Comparison with Nonlinear Potential Flow

In Ref. 3, a conical relaxation technique was applied to the nonlinear supersonic potential flow equation using shock-capturing techniques. Figure 15 shows some comparisons between the nonlinear potential flow solutions and the rotational Euler equations. Overall good agreement is achieved in most cases with the largest difference occurring locally around the leeward leading edge. The potential flow solution generally predicts lower pressures, thus higher crossflow Mach numbers in this vicinity. The shock positions are within reasonable agreement with the Euler solutions, having a tendency to predict shock locations slightly inboard of the potential flow solutions. This may be due to the nonconservative nature of the potential flow solutions.

Three-Dimensional Wing

Some preliminary results were obtained for three-dimensional wings.

A program that met the general requirements of geometrical continuity and detail mandatory to the finite-difference program is described in Ref. 14 and uses the basic bicubic surface patch theory of Ref. 15. Unlike methods that model wings using flat panels for linearized potential flow panel programs, this method panels the wing with nonlinear surface panels satisfying first-derivative continuity requirements at the panel boundaries.

A sample three-dimensional wing was then modeled with an 18.39 deg planform angle. It began with an initial conical section corresponding to a 6:1 ellipse at $Z = 30$. The centerline thickness of the wing was parabolic in nature resulting in a thin wing cross section at the trailing edge. The wing model also included camber and variation of cross-sectional thickness character. The wing was started with the converged Euler solution for the 6:1 ellipse at $M_\infty = 1.97$ and $\alpha = 10$ deg.

Figure 16 shows a nondimensionalized overlay of some of the cross-sectional shapes and pressure distributions. The parabolic nature of the centerline thickness causes a continuous expansion and shift in cross-sectional pressures which become distorted by the effect of cambering. The location of the shock did not change very much, moving slightly inboard. The expansion around the leading edge became quite large as

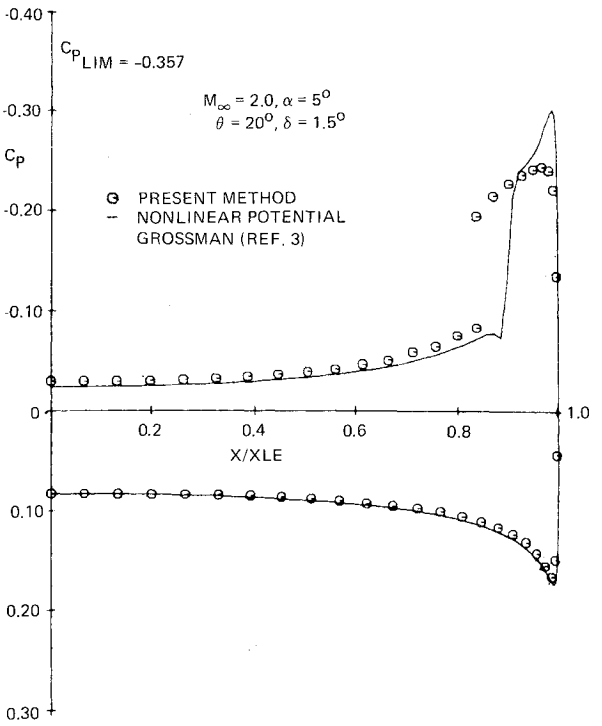

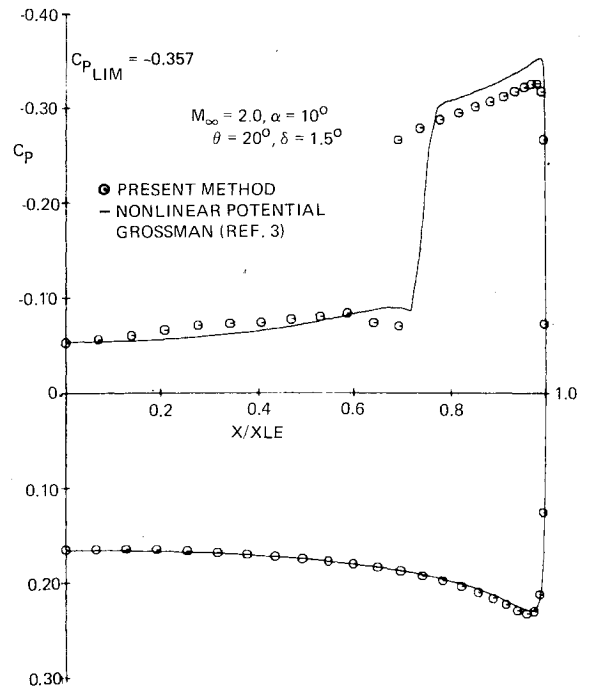

Fig. 15 Comparison of nonlinear methods, rotational vs irrotational.

the radius of curvature of the leading edge decreased with the thinner sections of the wing near the trailing edge. The limiting pressure coefficient at $M_\infty = 1.97$ is -0.368. It can be seen that the pressures approach but do not exceed this number as the sections become thinner. It must be mentioned at this point that most of the numerical procedures mentioned earlier and used for conical flow were relaxed for three-dimensional flow. The entropy generated by the crossflow shock on the body was allowed to propagate naturally to the leeward symmetry plane. The entropy at the saddle point was extrapolated from the incoming stagnation streamline and was allowed to propagate naturally on the body toward the windward and leeward planes. Figure 17 shows a plot of the crossflow Mach number for the same cross sections. It is

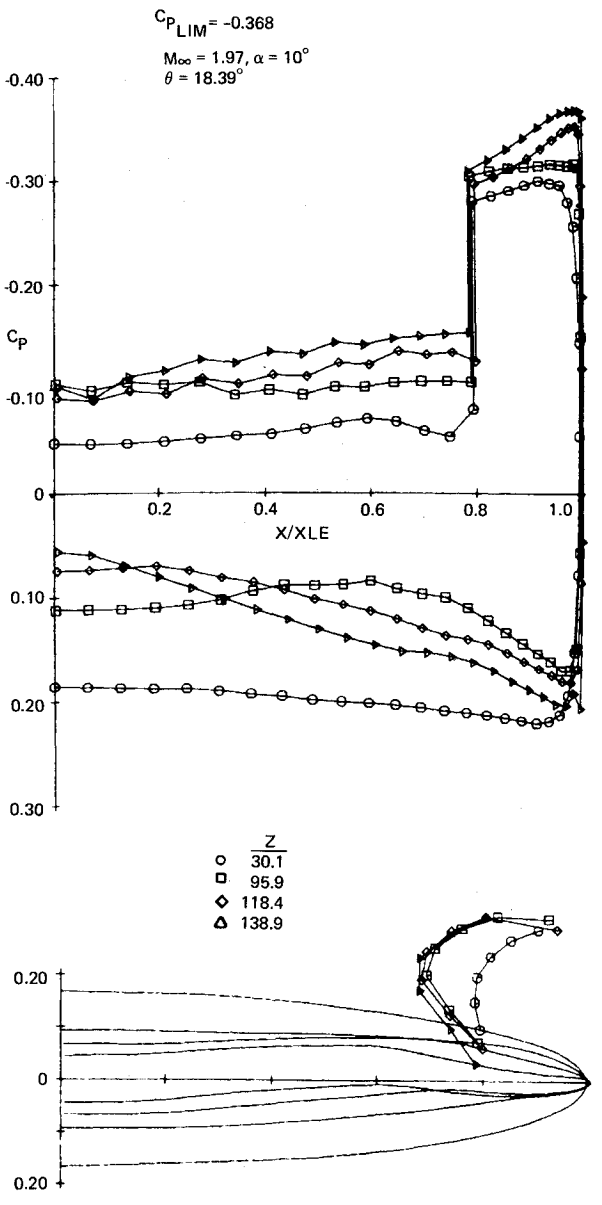

Fig. 16 Nondimensional surface pressure distributions and crossflow shocks for a three-dimensional wing, $M_\infty = 1.97$, $\alpha = 10$ deg.

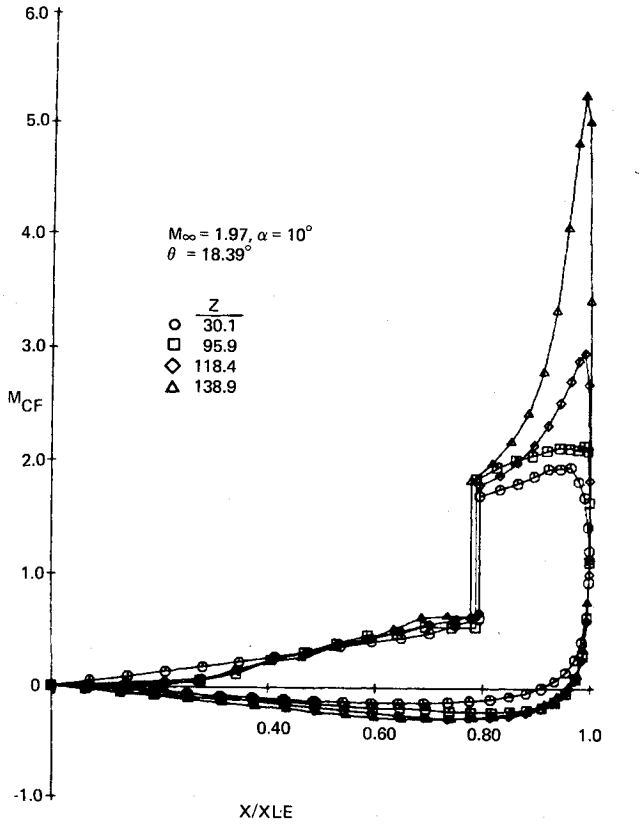

Fig. 17 Crossflow Mach number distributions for three-dimensional wing, $M_\infty = 1.97$, $\alpha = 10$ deg.

readily apparent that as the leading-edge radius becomes small, the expansion around the leading edge becomes enormous. For the thinner section, the crossflow Mach number approaches a value of 6.

Of course, these Mach numbers would be unattainable in a viscous flow, because leading edge separation would occur long before these solutions would exist. The shape and distortion of the crossflow shock and sonic line is interesting. The large expansion increases the size of the supersonic bubble and bends the crossflow shock in toward the symmetry plane, yet the body shock position remains only slightly altered from the original conical shock position. This is somewhat unexplainable since it would be expected that a conical shock generated by one of these thin sections would indeed lie inboard, as indicated by the movement of the field shock points. The crossflow Mach number on the body develops a slight gradient between the crossflow shock and symmetry plane. The entropy also develops a gradient in this region corresponding to the stronger shock developed by the thinner cross section and the initial starting value at the symmetry plane. These gradients probably explain the pressure oscillations that occur in this region.

Concluding Remarks

A finite-difference approach to solving the rotational Euler equations, explicitly fitting shocks as a boundary, has been successfully applied to a wide variety of geometric shapes in the lower supersonic Mach number regime. A variety of numerical difficulties was encountered with the conical flow problem that was primarily associated with the initial value characteristics of the hyperbolic scheme causing embedded shock-induced entropy and crossflow layers to develop on the body surface. Special techniques were adopted based on the physics of the flow in order to circumvent these difficulties.

It was also shown how the lower supersonic Mach number ($M_\infty \sim 2$), subsonic leading-edge wing poses a difficult problem from a numerical point of view. Smaller regions of embedded supersonic crossflow occur relative to the coordinate mesh with decreasing freestream Mach numbers. This results in large gradients in the vicinity of the body surface which are difficult to resolve numerically without a large number of grid points or a special coordinate stretching in this region.

During the course of the study, numerical efficiency was not a consideration and no attempts were made in this direction. All flowfields were computed on a fixed maximum mesh of 40 radial and 50 circumferential mesh points. Computer times for conical flow solutions ranged from 1 to 2 h on an IBM 370/168.

Acknowledgment

The author gratefully acknowledges the support and guidance of F. Marconi without whose support the present study would not have been possible and also the support of B. Grossman of the Research Department.

References

[1]Brown, C., McLean, F., and Klunker, E., "Theoretical and Experimental Studies of Cambered and Twisted Wings Optimized for

Flight at Supersonic Speeds," International Congress of Aeronautical Sciences, Madrid, Spain, 1960.

[2]Marconi, F. and Siclari, M. J., "A Study of the Inviscid Flow About Conically Cambered Delta Wings," AIAA Paper 78-58, Huntsville, Ala., 1978.

[3]Grossman, B., "Numerical Procedure for the Computation of Irrotational Conical Flows," *AIAA Journal*, Vol. 17, Aug. 1979, pp. 828-837.

[4]Ferri, A., "Supersonic Flow Around Circular Cones at Angle of Attack," NACA TN 2236, Nov. 1950.

[5]Klunker, E. B., South, J. C., and Davis, R. M., "Calculation of Nonlinear Conical Flows by the Method of Lines," NASA TR R-374, Oct. 1971.

[6]Kutler, P. and Lomax, H., "A Systematic Development of the Supersonic Flow Fields over and Behind Wings and Wing-Body Configurations Using a Shock-Capturing Finite-Difference Approach," AIAA Paper 71-99, New York, N.Y., Jan. 1971.

[7]Rakich, J. V. and Kutler, P., "Comparison of Characteristics and Shock Capturing Methods with Application to the Space Shuttle Vehicle," AIAA Paper 72-191, San Diego, Calif., Jan. 1972.

[8]Fletcher, C. A. J., "Vortical Singularity Behind a Highly Yawed Cone," *AIAA Journal*, Vol. 13, Aug. 1975, pp. 1073-1078.

[9]Daywitt, J., Anderson, D., and Kutler, P., "Supersonic Flow About Circular Cones at Large Angles of Attack, A Floating Discontinuity Approach," AIAA Paper 77-86, 1977.

[10]Moretti, G., Grossman, B., and Marconi, F., "A Complete Numerical Technique for the Calculation of Three Dimensional Inviscid Supersonic Flows," AIAA Paper 72-192, San Diego, Calif., Jan. 1972.

[11]Marconi, F., Salas, M., and Yaeger, L., "Development of a Computer Code for Calculating the Steady Super/Hypersonic Inviscid Flow Around Real Configurations," NASA CR 2675, 1976.

[12]Melnik, R. E., "Vortical Singularities in Conical Flow," *AIAA Journal*, April 1967, pp. 631-637.

[13]Mason, W., private communication.

[14]Craidon, C. B., "A Computer Program for Fitting Smooth Surfaces to an Aircraft Configuration and Other Three-Dimensional Geometries," NASA TM X 3206, June 1975.

[15]Coons, S. A., "Surface for Computer-Aided Design of Space Forms," MAC-TR-41 (Contract No. AF-33(600)-42859), MIT, June 1967.

[16]Ferrari, C. and Tricomi, F. G., *Transonic Aerodynamics*, Academic Press, New York, 1968.

[17]Siclari, M. J. and Marconi, F., "Analysis and Design of Supersonic Aircraft Based on Nonlinear Eulerian Equations," AFFDL TR (to be published), USAF-FDL Contract F33615-77-C-3126.